Neurobiology of Disease 132 (2019) 104581

Contents lists available at ScienceDirect

Neurobiology of Disease

journal homepage: www.elsevier.com/locate/ynbdi

Perturbations in RhoA signalling cause altered migration and impaired neuritogenesis in human iPSC-derived neural cells with PARK2 mutation

Helle Bogetofte[a,b], Pia Jensen[c], Justyna Okarmus[a], Sissel Ida Schmidt[a], Mikkel Agger[a], Matias Ryding[a], Peter Nørregaard[a], Christina Fenger[a], Xianmin Zeng[d], Jesper Graakjær[e], Brent James Ryan[b], Richard Wade-Martins[b], Martin Røssel Larsen[c], Morten Meyer[a,f,*]

[a] Department of Neurobiology Research, Institute of Molecular Medicine, University of Southern Denmark, J.B. Winsloews Vej 21, st, DK5000 Odense C, Denmark
[b] Oxford Parkinson's Disease Centre, Department of Physiology, Anatomy and Genetics, South Parks Road, University of Oxford, OX1 3QX Oxford, UK
[c] Department of Biochemistry and Molecular Biology, University of Southern Denmark, Campusvej 55, DK5230 Odense M, Denmark
[d] Buck Institute for Research on Ageing, 8001 Redwood Boulevard, Novato, CA 94945, USA
[e] Department of Clinical Genetics, Vejle Hospital, Kabbeltoft 25, 7100 Vejle, Denmark
[f] BRIDGE, Brain Research – Inter-Disciplinary Guided Excellence, Department of Clinical Research, University of Southern Denmark, J.B. Winsloews Vej 19, DK5000 Odense C, Denmark

ARTICLE INFO

Keywords:
Parkinson's disease
iPSCs
Isogenic
Proteomics
Post-translational modifications
Neurite outgrowth
Cell migration
RhoA signalling

ABSTRACT

Mutations in parkin, encoded by the *PARK2* gene, causes early-onset familial Parkinson's disease (PD), but dysfunctional parkin has also been implicated in sporadic PD. By combining human isogenic induced pluripotent stem cells (iPSCs) with and without *PARK2* knockout (KO) and a novel large-scale mass spectrometry based proteomics and post-translational modification (PTM)-omics approach, we have mapped changes in protein profiles and PTMs caused by parkin deficiency in neurons. Our study identifies changes to several proteins previously shown to be dysregulated in brains of sporadic PD patients. Pathway analysis and subsequent *in vitro* assays reveal perturbations in migration and neurite outgrowth in the *PARK2* KO neurons. We confirm the neurite defects using long-term engraftment of neurons in the striatum of immunosuppressed hemiparkinsonian adult rats. The GTP-binding protein RhoA was identified as a key upstream regulator, and RhoA activity was significantly increased in *PARK2* KO neurons. By inhibiting RhoA signalling the migration and neurite outgrowth phenotypes could be rescued. Our study provides new insight into the pathogenesis of PD and demonstrates the broadly applicable potential of proteomics and PTMomics for elucidating the role of disease-causing mutations.

1. Introduction

Mitochondrial dysfunction and oxidative stress are key contributing factors in the etiology of Parkinson's disease (PD), particularly affecting the more vulnerable dopaminergic neurons of the substantia nigra pars compacta (SNpc) (Abou-Sleiman et al., 2006; Dias et al., 2013). Several familial forms of PD are caused by loss-of-function mutations in the genes encoding parkin (*PARK2*), PINK1 (*PARK6*), and DJ-1 (*PARK7*) (Lücking et al., 2000; Bonifati et al., 2003; Valente et al., 2004), which are all important for mitochondrial homeostasis (Abou-Sleiman et al., 2006; Exner et al., 2012). Parkin is an ubiquitin E3 ligase, which is recruited to depolarised mitochondria, where it ubiquitinates proteins to initiate removal of the damaged mitochondria by selective autophagy (mitophagy) (Narendra et al., 2008). Parkin dysfunction has also been demonstrated in sporadic PD underlining the relevance of genetic parkin disease models in research of both sporadic and familial PD (Dawson and Dawson, 2014). However, *Park2* knockout (KO) rodents display overall mild and variable phenotypes with mitochondrial dysfunction, increased oxidative stress, changes in dopamine metabolism and limited signs of the classic pathological hallmarks of PD (Kitada et al., 2009; Oliveras-Salvá et al., 2011; Sliter et al., 2018). This highlights the need for a better model of parkin loss of function in PD and a better understanding of how PARK2 dysfunction mediates PD.

Induced pluripotent stem cells (iPSCs), derived from somatic cells, have enabled investigation of the progressive development of disease relevant cellular changes in human dopaminergic neurons from PD patients (Fernandes et al., 2016; Mazzulli et al., 2016). Concurrently, the advancement of genome editing techniques has allowed us to

* Corresponding author at: Department of Neurobiology Research, Institute of Molecular Medicine, University of Southern Denmark, Winsloewparken 21, st, DK-5000 Odense C, Denmark.
E-mail address: mmeyer@health.sdu.dk (M. Meyer).

https://doi.org/10.1016/j.nbd.2019.104581
Received 28 January 2019; Received in revised form 30 July 2019; Accepted 20 August 2019
Available online 21 August 2019

introduce or correct disease-causing mutations in PD relevant genes of importance for mitochondrial function. Isogenic iPSC lines facilitate the examination of isolated effects of mutant PD-relevant proteins, including parkin, in developing and newly formed human neurons (Soldner et al., 2011; Shaltouki et al., 2015).

Studies of PD patient iPSC-derived neurons harbouring various *PARK2* mutations have documented increased oxidative stress, abnormal mitochondrial morphology and function, dysregulation of dopamine homeostasis, and α-synuclein accumulation (Jiang et al., 2012; Imaizumi et al., 2012; Chung et al., 2016). Moreover, one study found that *PARK2* mutations caused reduced complexity of the neuronal cell processes (Ren et al., 2015). This is thought to be a result of parkin's role in ubiquitination and degradation of misfolded tubulins and stabilization of microtubules (Yang et al., 2005; Ren et al., 2003). However, the downstream consequences leading to cell death and the relevance of these pathways for sporadic PD remain unresolved.

Unbiased proteomic analyses have been applied to human post-mortem brain tissue to identify large numbers of proteins affected in PD (Werner et al., 2008; Licker et al., 2014). However, large-scale studies of post-translational protein modification (PTMs) such as phosphorylation (Larsen et al., 2005; Engholm-Keller et al., 2012) and cysteine-modifications (Huang et al., 2016), which are essential for regulating activity and function of proteins and cellular pathways have not been reported (Ren et al., 2014). Parkin activation following mitochondrial depolarisation requires phosphorylation of both parkin and ubiquitin by PINK1, which also causes changes in phosphorylation states of several downstream targets (Lai et al., 2015). Interestingly, PTMs such as phosphorylation impacts the aggregation and clearance of key PD-associated proteins, including α-synuclein and tau (Tenreiro et al., 2014; Barrett and Timothy Greenamyre, 2015). Less well characterized is the importance of cysteine-modifications. Oxidative PTMs of the thiol group in cysteine residues can function as reversible redox switches to regulate protein structure, activity and localization. Oxidative stress is a key contributor to PD and cysteine thiol groups of proteins are particularly susceptible to oxidative modifications by oxygen, nitrogen and sulfur species (Fang et al., 2007; Danielson et al., 2011; Garcia-Garcia et al., 2012). Oxidative modifications of cysteines in PD-related proteins such as parkin, DJ-1 and ubiquitin carboxyl-terminal hydrolase L1 (UCHL1) are found at increased levels in sporadic PD patients (Choi et al., 2004; Wang et al., 2005; Saito, 2014).We have recently developed a workflow, which enable the study of global changes in PTM-omics by simultaneous enrichment of phosphorylated peptides and peptides with reversible cysteine modifications (Huang et al., 2016).

In the present work we have applied this workflow to allow us for the first time to identify and quantify a large number of dysregulated proteins and PTMs including phosphorylation and reversible cysteine-modifications in human iPSC-derived neurons with compound heterozygous *PARK2* mutations (Huang et al., 2016). Many of the proteins most highly affected in the *PARK2* KO neurons are known from the literature to be comparably altered in sporadic PD brains. This supports the existence of common pathways shared between familial *PARK2*-related- and sporadic PD. In addition our analysis identified changes in several proteins and pathways, which are more novel in a PD context, including factors affecting cell migration and neurite outgrowth. These we were able to confirm by functional assays *in vitro* and *in vivo* by grafting iPSC-derived neuronal precursors into the striatum of hemiparkinsonian rats, hereby emphasizing the physiological relevance of the observed phenotypes.

The GTP-binding protein RhoA, which regulates both cell migration and neurite outgrowth, has been implicated in dopaminergic neurodegeneration in various animal models (Labandeira-Garcia et al., 2015). Our analysis identified increased RhoA signalling as an important upstream regulator, and by inhibiting this pathway, we could rescue the observed phenotypic changes, highlighting the potential of this novel approach.

2. Results

2.1. PARK2 mutation does not affect neuronal differentiation

Mutations in the *PARK2* gene are known to cause PD, but the exact mechanisms through which this happens are unknown. To explore the pathogenesis of PD, we utilized two isogenic iPSC lines created from a healthy control iPSC line, where deletions have been introduced in exon 2 on both alleles of the *PARK2* gene by genome editing. The cell lines pluripotency, normal karyotype and *PARK2* genotype have previously been established (Shaltouki et al., 2015). To ascertain that the iPSCs had not acquired unwanted genetic differences in culture, we confirmed their normal karyotype by single nucleotide polymorphism (SNP) array (Fig. S1A). The presence of the compound heterozygous mutations in the *PARK2* KO line was verified by quantitative real time polymerase chain reaction (qRT-PCR) on genomic DNA for the wild type (wt) *PARK2* exon 2 sequence, which was present in control and not in *PARK2* KO iPSCs (Fig. S1B). Western blotting for the parkin protein confirmed the KO (Fig. S1C). Immunofluorescence (IF) demonstrated that the iPSCs were positive for the established pluripotency markers OCT4 and SOX2 (Figs. S1D-E), whereas neural stem cell (NSC) lines differentiated from these expressed the NSC markers Nestin and SOX2 (Figs. S1F–H).

The NSCs were differentiated for 25 days resulting in cultures with a large percentage of β-tubulin-III (TUJ1)+ (control: 86.4 ± 1.0%, *PARK2*: 85.5 ± 0.6%) and tyrosine hydroxylase (TH)+ neurons (control: 25.1 ± 1.6%, *PARK2*: 26.2 ± 4.0%) (Figs. 1A, E–F).

A large part of the neurons were mature as shown by the proportion of microtubule associated protein 2 (MAP2)+ cells (control: 67.9 ± 0.9%, *PARK2*: 65.1 ± 2.5) and also the presence of clusters of NeuN+ neurons (Figs. 1B–C, G). GABAergic neurons, which are present in midbrain dopaminergic nuclei including the substantia nigra (SN) pars reticularis (Morello and Partanen, 2015), were also found in the cultures (control: 27.6 ± 4.9%, *PARK2*: 33.8 ± 2.0%) (Fig. 1D, H). Control and *PARK2* KO neurons contained equal amounts of all markers (Fig. 1E–H) and total cell numbers were similar (control: 1396 ± 139, *PARK2*: 1208 ± 20 cells/mm^2) (Fig. 1I). Based on this, we concluded that the *PARK2* KO and wt control iPSC lines had similar capacity for generating midbrain dopaminergic neuronal cultures.

2.2. Mass spectrometry identifies dysregulated proteins related to Parkinson's disease (PD)

To gain new insights into the role of *PARK2* dysfunction in PD, we applied a mass spectrometry based proteomics and PTMomics strategy, which allowed us to explore both protein and post-translational modifications (PTMs) changes in *PARK2* KO and isogenic control neurons. This method successfully identified and quantified a large number of proteins and PTMs including phosphorylation and cysteine-modifications (Figs. J-K, Fig. S2A). Data are available *via* ProteomeXchange Consortium *via* the PRIDE partner repository with the identifier PXD007871.

A total of 98 proteins showed significantly altered expression levels in the proteomics analysis of *PARK2* KO neurons compared to controls (Fig. 1K). Several of the most up- and down-regulated proteins have already been associated with PD pathogenesis (Fig. 2A, Fig. S2C). Galectin-1 (LGALS1) and glial fibrillary acidic protein (GFAP) (Fig. 2A) as well as ferritin H and L (Table S1A) are all up-regulated in SN of PD patients (Werner et al., 2008).

The increased GFAP level was confirmed by Western blotting (Fig. 2B, Fig. S6), and immunofluorescence microscopy revealed a small but significant (control: 7.2 ± 0.3%, *PARK2*: 8.1 ± 0.1%, $p < .05$) increase in the number of GFAP+ astrocytes in *PARK2* KO cultures (Fig. 2G–H). The astrocytes were generally more intensely stained and of a larger size in the *PARK2* KO cultures compared to controls (Fig. 2G). In addition, another marker for reactive astrocytes, vimentin,

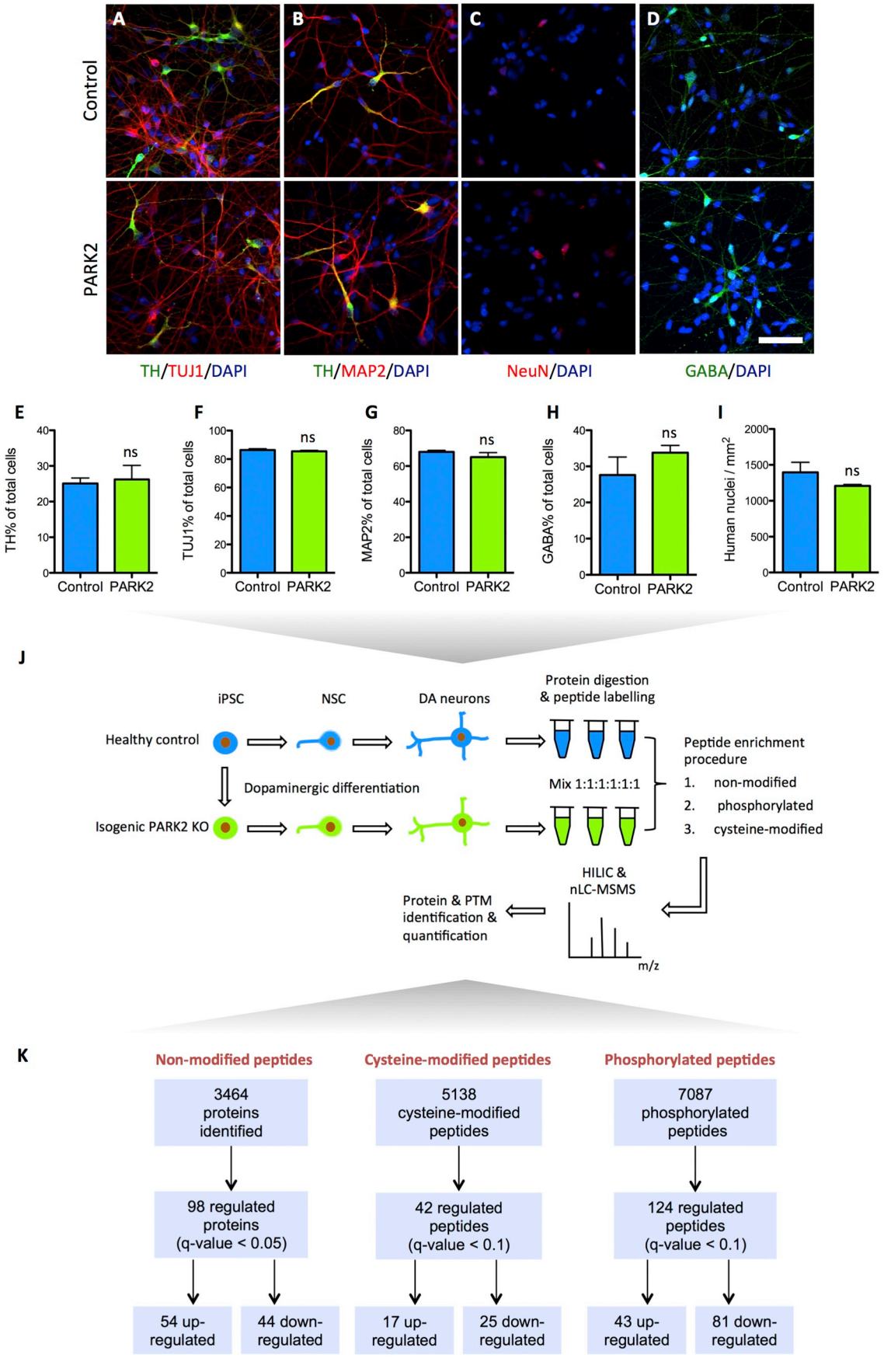

(caption on next page)

Fig. 1. Identification of differentially expressed proteins and post-translational modifications (PTMs) in *PARK2* knockout (KO) neurons compared to isogenic controls.
(A–I) Immunofluorescence staining and quantification of control and *PARK2* KO neurons on differentiation day 25 showed no differences in levels of (A, E, F) tyrosine hydroxylase (TH, green) and β-tubulin-III (TUJ1, red): $N = 3$ independent differentiations, (B, G) TH (green) and microtubule-associated protein 2 (MAP2, red): N = 3 independent differentiations, (C) neuronal nuclei (NeuN, red), (D, H) γ-aminobutyric acid (GABA, green): N = 3 technical replicates, and (I) total cell numbers (DAPI + nuclei, blue) per mm^2: $N = 5$ independent differentiations. Scale bar = 50 μm. Mean ± SEM (J) Overview of the experimental set-up: proteins from *PARK2* KO and isogenic control neuronal cultures from three independent differentiation were digested to peptides and labeled prior to the peptide enrichment procedure separating phosphorylated and cysteine-modified peptides from the remaining "non-modified" peptides. Using hydrophilic interaction liquid chromatography (HILIC) and nano-liquid chromatography tandem mass spectrometry (nLC-MSMS) the peptides and PTMs were identified and quantified (K) Overview of the identified non-modified proteins (> 1 unique peptide) and phosphorylated/cysteine-modified peptides (normalized to protein level). Levels of 98 proteins, 42 cysteine-modified peptides and 124 phosphorylated peptides were significantly altered in *PARK2* KO neurons using Rank products with a q-value (FDR-adjusted *p*-value) cut-off of 0.05 for proteins and 0.10 for PTMs. (For interpretation of the references to colour in this figure legend, the reader is referred to the web version of this article.)

was also up-regulated in *PARK2* KO cultures as shown by Western blotting (Fig. 2I, Fig. S6).

Synapsin III levels, which were confirmed by Western blotting to be increased (Fig. 2C, Fig. S6), are also augmented in PD patient brains (Zaltieri et al., 2015). Interestingly, the synapsin III phosphorylation levels were markedly decreased at several known phosphosites including S470, which is important for neurotrophic signalling (Table S1B) (Porton et al., 2011).

Down-regulation of microtubule-associated protein light chain 3A (LC3A) as well as the LC3B isoform was confirmed by Western blotting (Fig. 2D–E, Fig. S6) and indicates changes in autophagy, a key pathway in PD pathogenesis (Beilina and Cookson, 2016). Moreover, catalase, an important enzyme in cellular defence against oxidative stress, was decreased in *PARK2* KO neurons, which was confirmed by Western blotting (Fig. 2F, Fig. S6). Decreased catalase activity has been demonstrated in the SN of PD patients (Ambani et al., 1975).

Pathway analysis of the 98 dysregulated proteins indicated an enrichment of proteins related to neurological disease including movement disorders, disorder of the basal ganglia and neurodegeneration. Cell death and survival including neuronal cell death and cell viability were similarly highlighted, as were more novel areas such as cell morphology, cellular movement, −assembly and −organisation (Fig. S3).

Overall these findings underline the ability of our approach to identify PD-related protein changes.

2.3. Pathway analysis reveals overall changes affecting cell migration and neuritogenesis

In addition to identifying a large number of dysregulated proteins, our approach also resulted in the first ever characterization of changes in phosphorylation and reversible cysteine-modifications in human *PARK2* KO neurons, providing a valuable resource for future studies (Table S1B–C).

Significant PTM level changes were found at 124 phospho-sites and 42 cysteine-residues on 101 and 36 proteins, respectively (Fig. 1K, Fig. S2B).

Pathway analysis of the cysteine-modified proteins showed a significant enrichment of proteins involved in PD-related pathways such as protein ubiquitination, unfolded protein response and mitochondrial dysfunction (Fig. 3A). A total of 5 out of the 36 proteins were of importance for axonal guidance signalling. Protein ubiquitination was similarly highlighted amongst the phosphorylated proteins, which also showed an enrichment of proteins related to actin cytoskeleton signalling including cdc42- and RhoA signalling (Fig. 3A).

To fully integrate our proteomics and PTMomics data, we performed a cross-comparison to identify the functions and pathways, which were most highly enriched across the three datasets (Fig. 3B). Levels and PTMs of proteins of relevance for morphology and development of neurons, cell migration, neuritogenesis and quantity of calcium amongst others were highly affected in *PARK2* KO neurons (Fig. 3B). Consistent with this, changes were predicted in a number of canonical pathways (Fig. 3A), which can affect several of the identified functions. Phosphatidylinositide 3-kinase (PI3K)/Akt-, Ephrin- and Rho GTPase signalling, including the two Rho GTPase family members RhoA- and Cdc42 (Fig. 3A), are important for regulation of neuronal cell morphology, migration and neuritogenesis (Stankiewicz and Linseman, 2014; Takeuchi et al., 2015).

Overall, the pathway analysis of both protein and PTM changes enabled the identification of a number of known and novel pathways and function, which based on the proteomic analysis were affected by parkin dysfunction.

2.4. PARK2 KO neurons exhibit neurite outgrowth deficits in vitro and in vivo

Perturbations in neurite morphology and maintenance have previously been documented as a result of PD-related mutations. Based on the pathway analysis a number of proteins as well as phosphorylated and cysteine-modified proteins of importance for neuritogenesis were affected in the *PARK2* KO neurons (Fig. 4A). We therefore sought to further functionally validate these changes and investigate neurite outgrowth *in vitro* in our differentiating *PARK2* KO and control cultures, specifically focusing on the dopaminergic subset. As predicted, the *PARK2* KO TH + neural precursors had significantly fewer neurites per cell (control: 2.4 ± 0.0, *PARK2*: 1.7 ± 0.1, $p = .008$) and the neurites were significantly shorter (control: 212.1 ± 16.4, *PARK2*: 153.2 ± 6.4, $p = .044$) (Fig. 4B, D, F). The number of branch points was not significantly decreased (control: 1.2 ± 0.2, *PARK2*: 0.7 ± 0.1, $p = .050$) (Fig. 4B, E).

We next sought to determine whether these differences were temporary or would be sustained after long-term culture. For this purpose, control and *PARK2* KO neural precursors were differentiated for 16–17 days and transplanted into striatum of hemiparkinsonian, 6-hydroxydopamine (OHDA)-lesioned, immunosuppressed adult rats (Fig. S4A). The rats had been stratified into two groups ($n = 16$ rats per group) with similar lesion severity based on amphetamine-induced rotations scores. Remaining cells from the transplantation cell suspensions were replated through the Hamilton microsyringe used for the transplantation to assess if the procedure affected the survival of the two cell lines differently. However, no differences in total cell number or percentage of β-tubulin-III + and TH + cells were observed when the cells were fixed and immunostained the following day (Fig. S4B-D). At 16 weeks postgrafting, brains were isolated and processed histologically to evaluate the number of surviving cells, the presence of mature MAP2 + neurons, the percentage- and morphology of TH + cells in the grafts. Four rats, one from the control and three from the *PARK2* KO group, had no visible grafts and were excluded from the analysis. The remaining 28 rats all contained striatal grafts with HN + cells (control: 598.1 ± 98.1 *PARK2*: 640.6 ± 163.3 per section) and extensive MAP2 immunostaining, although the average number of HN + cells per graft was quite variable (Fig. 4G, I). The number of TH + cells appeared lower in the *PARK2* KO group, although only near significant (control: 15.4 ± 4.2, *PARK2*: 5.8 ± 1.4 per section, $p = .051$) (Fig. 4G, J–K).

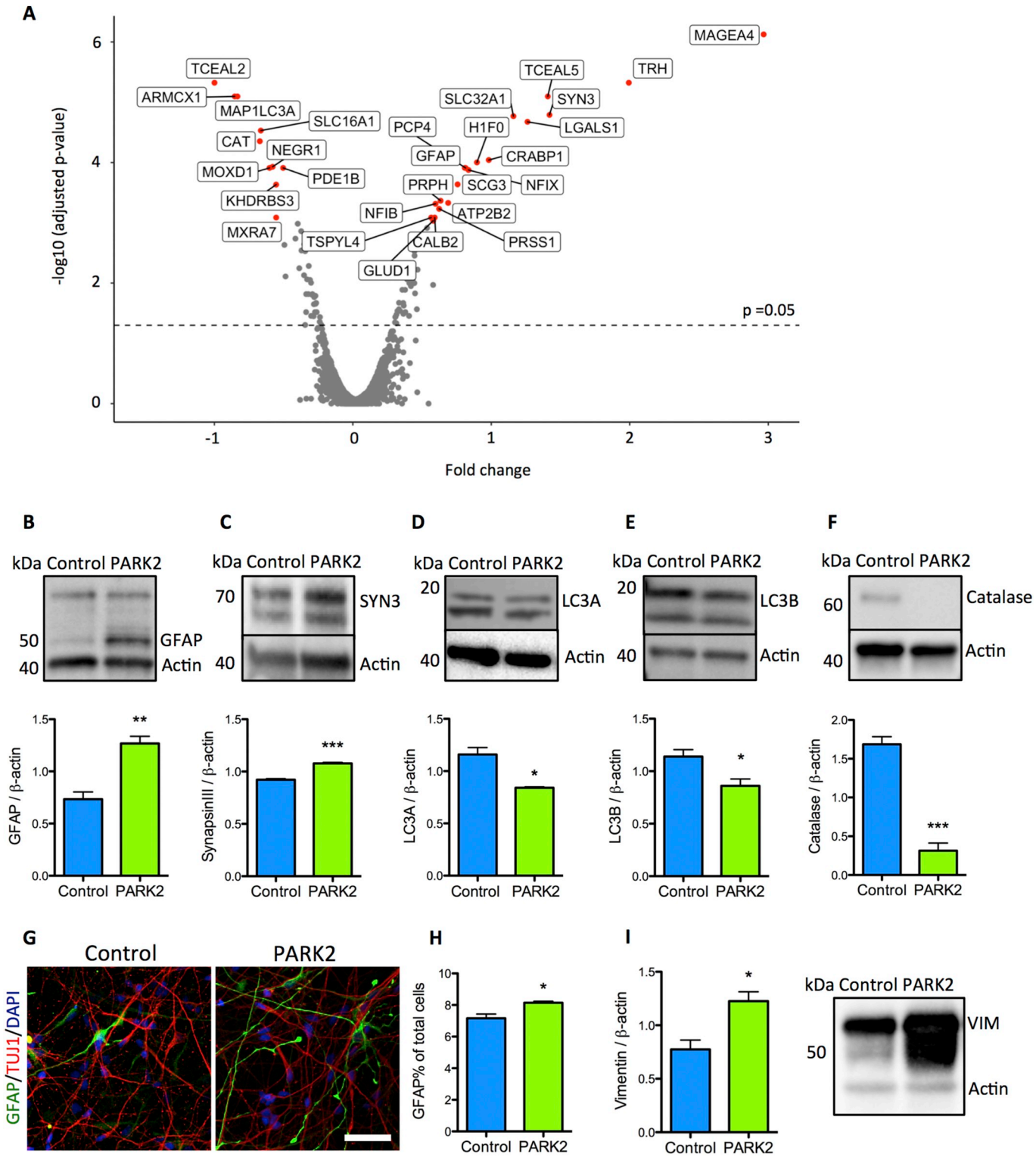

Fig. 2. Western blotting confirmed changes in top up- and down-regulated proteins identified by mass spectrometry.
(A) Volcano plot showing the fold change and significance level (−log10 (FDR-adjusted p-value)) of all proteins. The labeled proteins have a FDR-adjusted p-value < .001. (B–F) Western blotting confirmed significant changes in levels of (B) glial-acidic fibrillary protein (GFAP), (C) synapsin III (SYN3), (D-E) microtubule-associated protein light chain 3A and –3B (LC3A and LC3B), and (F) catalase in *PARK2* KO neurons. Expression levels were normalized to β-actin and shown relative to the average per differentiation. Mean ± SEM, $N = 3$ independent differentiations. (G) Immunofluorescence staining of control and *PARK2* KO neurons on day 25 for GFAP (green) and β-tubulin-III (TUJ1, red) showed larger, more intensely stained astrocytes in *PARK2* KO cultures. Cell nuclei were stained with DAPI (blue). Scale bar = 50 µm. (H) Quantification of GFAP immunofluorescence revealed a small, but significant difference in the relative content of GFAP+ cells. Mean ± SEM, $N = 3$ independent differentiations. (I) Increase in levels of the astrocytic marker vimentin in *PARK2* KO neurons, as assessed by Western blotting. Expression levels were normalized to β-actin and shown relative to the average per differentiation. Mean ± SEM, N = 3 independent differentiations, Students *t*-test. $^{*}P < .05$, $^{**}P < .01$, $^{***}P < .001$. (For interpretation of the references to colour in this figure legend, the reader is referred to the web version of this article.)

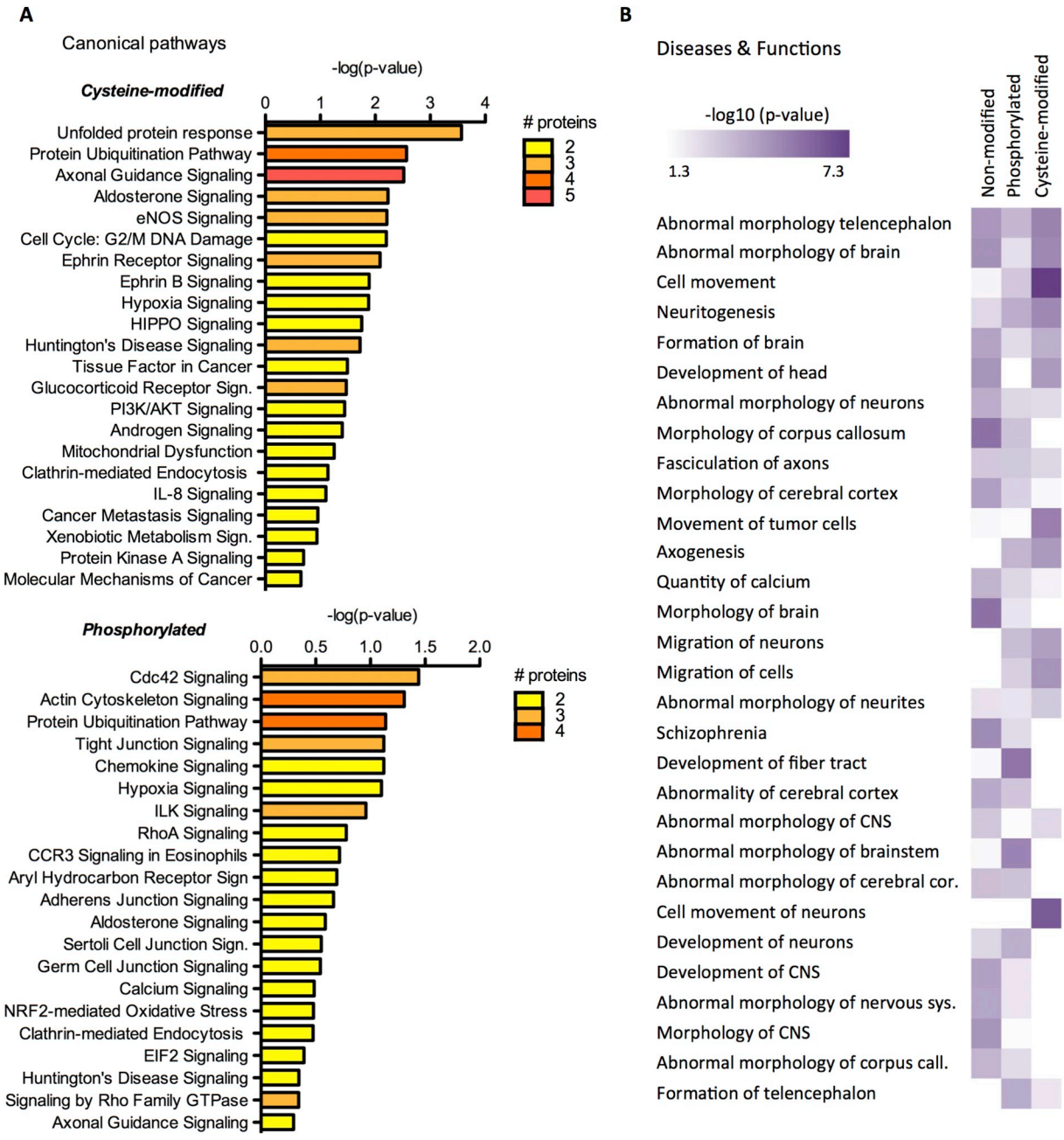

Fig. 3. Pathway Analysis predicts changes in cell migration, neurite outgrowth, and Rho GTPase signalling.
(A) Ingenuity Pathway Analysis (IPA) on the phosphorylated and cysteine-modified proteins showing the enrichment score (−log10 (p-value) and the number of identified proteins belonging to each pathway. Only pathways with two or more proteins are shown. (B) Comparison analysis was performed using IPA on all three datasets (non-modified, phosphorylated and cysteine-modified) from the proteomic characterization of *PARK2* knockout (KO) neurons. Data from the 30 most highly enriched diseases and functions are presented with a heat map of the enrichment scores (−log10 (p-value) for each dataset.

The morphology of the TH+ cells, however, was altered (Fig. 4H). While numbers of primary neurites per neuron were similar (control: 1.8 ± 0.1, *PARK2*: 1.5 ± 0.1) (Fig. 4L), the length of the neurites (control: 225.7 ± 16.3, *PARK2*: 141.7 ± 17.3 μM, $p = .002$) (Fig. 4M) and the number of branches per neuron (control: 1.6 ± 0.2, *PARK2*: 0.8 ± 0.2, $p = .016$) (Fig. 4N) was significantly decreased for grafts of *PARK2* KO dopaminergic neurons compared to isogenic controls, confirming that the neurite outgrowth defects caused by the *PARK2* mutation were persistent after a long-term survival *in vivo*. Combined with our *in vitro* data, we conclude that parkin deficiency leads to defects in neurite outgrowth, resulting in permanently decreased branching and neurite length.

2.5. Migration and neurite outgrowth changes in PARK2 KO neural precursors rescued by RhoA inhibition

Proteins involved in cell migration were highly enriched in the proteomics data, mainly amongst the proteins displaying differences in phosphorylation and reversible cysteine-modifications in *PARK2* KO neurons (Fig. 5A). Interestingly, RhoA signalling was identified as a potential causative pathway, mainly due to a significant enrichment of proteins involved in the RhoA signalling pathway with an altered phosphorylation state (Takeuchi et al., 2015; Surks et al., 2003; Parri et al., 2007; Hall and Lalli, 2010). These included one of the major downstream targets of the RhoA pathway, cofilin-1, which showed significantly increased phosphorylation levels corresponding with

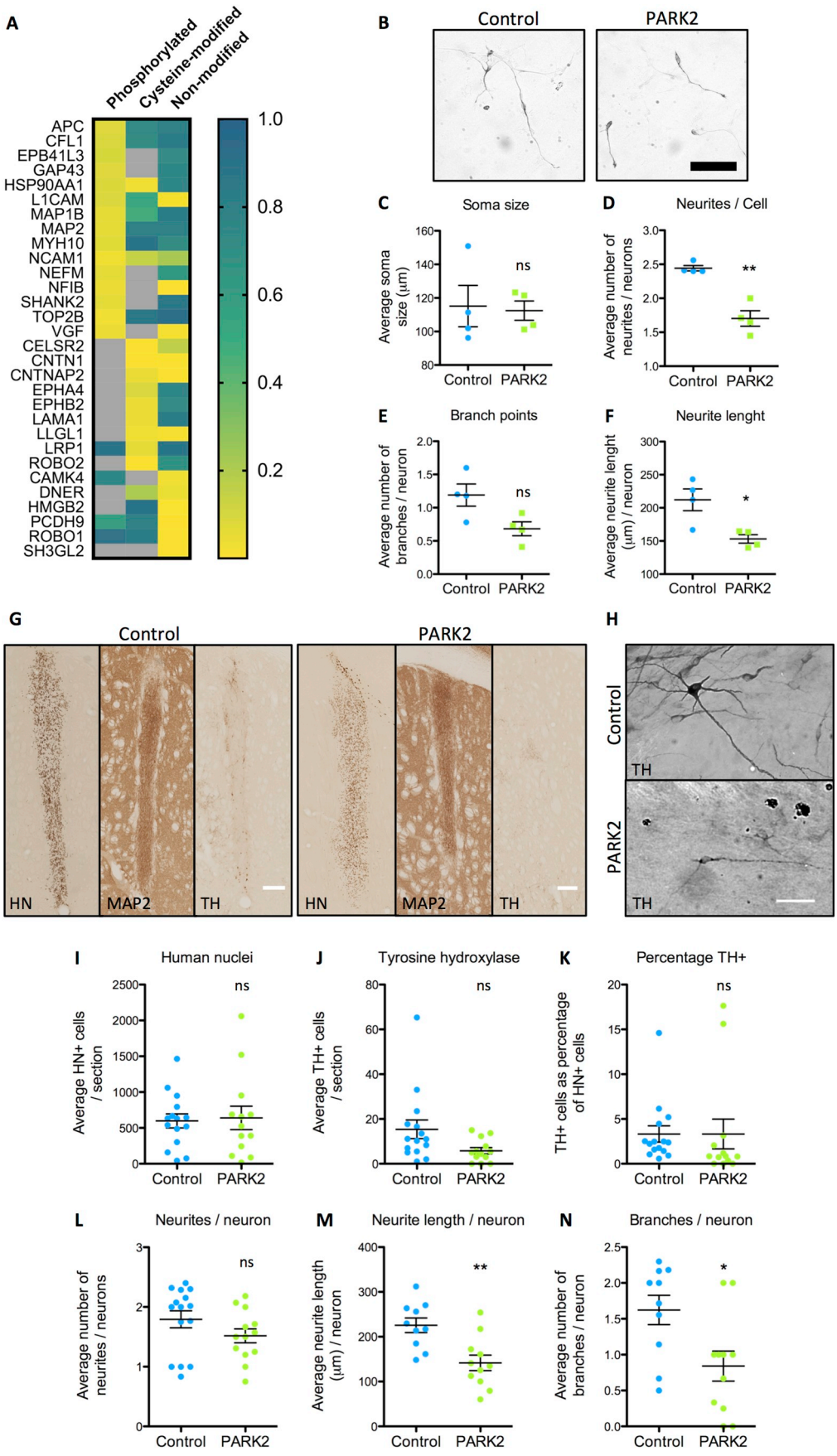

Fig. 4. Neurite outgrowth defects in *PARK2* knockout (KO) cells confirmed *in vitro* and after 16 weeks *in vivo*.
(A) Proteomics identified proteins of importance for neuritogenesis presented in a heat map of the q-values (FDR-adjusted *p*-values) representing whether the non-modified protein level or PTM levels were significantly altered in *PARK2* KO neurons compared to controls. Grey marks proteins, which were not identified amongst the phosphorylated or cysteine-modified. (B) Dopaminergic neuronal precursors identified in differentiation day 13 *PARK2* KO and isogenic control cultures using immunocytochemistry staining for tyrosine hydroxylase (TH). Scale bar = 100 µm. (C–F) Analysis of the morphology of TH+ dopaminergic neuronal precursors revealed no significant changes in (C) soma size (µm) or (D) branch points per cell, but significantly lower (E) average number of neurites per cell and significantly shorter (F) average neurite length per neuron (µm). Mean ± SEM, $N = 4$ wells (55–60 neurons), data from two independent differentiations. (G) Immunohistochemistry for human nuclei (HN), tyrosine hydroxylase (TH), and microtubule-associated protein 2 (MAP2) verified the presence of grafted human neurons in the rat striatum. One rat in the control group and three rats in the *PARK2* KO group contained no visible grafts and were excluded from further analysis. Scale bar = 200 µm. (H) Representative images of the morphology of the *PARK2* KO and isogenic control TH+ dopaminergic neurons in the grafts. Scale bar = 50 µm. (I–J) Numbers of HN+ and TH+ cells per brain section were similar between *PARK2* KO- and control-transplanted rats. (K) The relative content of TH+ cells was around 3.5% in both *PARK2* KO and control grafts. Mean ± SEM, control: $N = 15$, *PARK2*: $N = 13$. (L-N) Analysis of morphology of TH+ dopaminergic neurons revealed (L) similar numbers of neurites per neurons, and a significant decrease in (M) the average neurite length per neuron and (N) the average number of branches per neuron in *PARK2* KO grafts compared to control. Mean ± SEM, control: $N = 10$, *PARK2*: $N = 11$, grafts without TH+ neuron were excluded from the analysis, Student's t-test with Welch's correction. *P < .05, **P < .01, ***P < .001.

A

Proteins	PTM site	Ratio
Phosphorylated		
ADGRL3	T1445; S1446	1.49
APC	S2794	0.68
HSP90AA1	S231	0.67
CFL1	S3	1.48
L1CAM	S1243	1.37
MAP1B	S1462	1.48
	S561	0.46
	S614	1.52
MAP2	S1362	1.44
	S1679	0.68
MPRIP	S993	0.62
TOP2B	S1400; S1413	1.92
Cysteine-modified		
CELSR2	C1761	0.57
CNTNAP2	C1178	0.68
EPHB2	C272	0.69
HSP90AA1	C420	1.59
HSPA8	C574	1.41
PLXNA2	C701	0.7

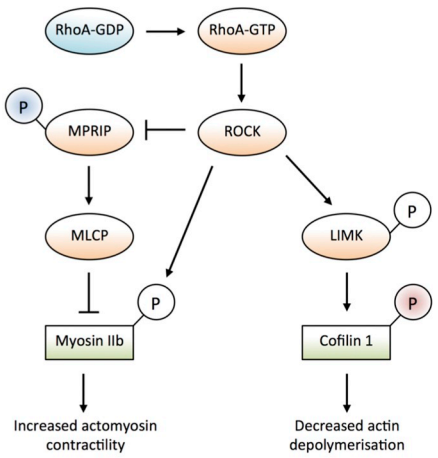

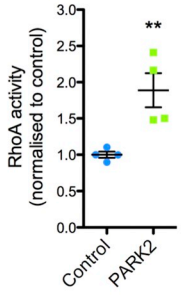

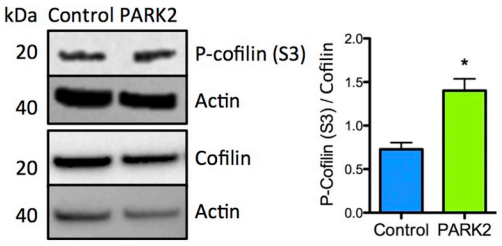

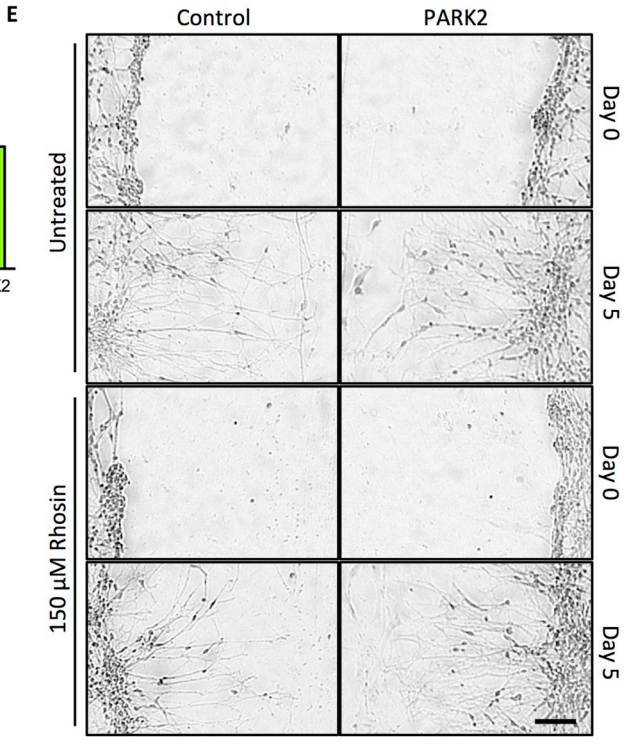

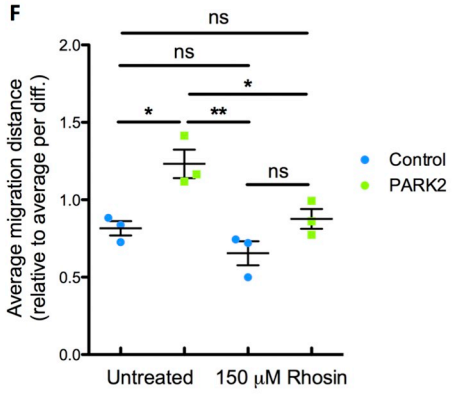

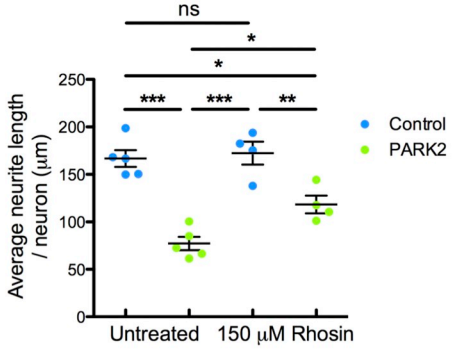

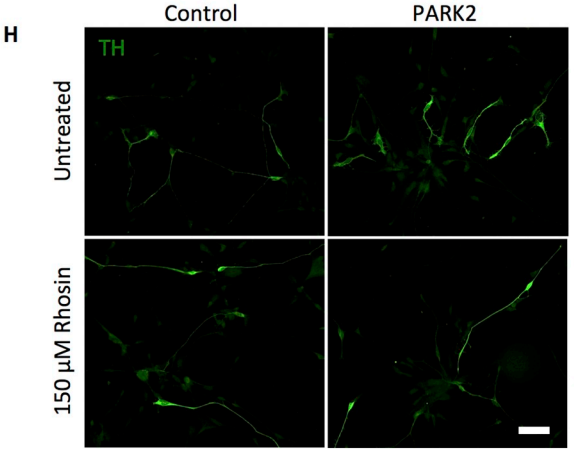

(caption on next page)

Fig. 5. RhoA inhibition rescued increased migration in *PARK2* knockout (KO) neurons and promoted neurite outgrowth.
(A) Table showing the proteins of importance for cell migration with significantly altered PTM levels in *PARK2* KO neurons. Listed are the specific PTM sites and the ratio of the modified peptides in *PARK2* KO neurons over controls. (B) Simplified schematic of the RhoA pathway: Active, GTP-bound RhoA signals through the effector Rho-associated kinase (ROCK), which *via* LIM kinase (LIMK) causes increased phosphorylation and inhibition of cofilin 1, leading to decreased actin polymerisation. ROCK signalling also leads to increased myosin IIb phosphorylation and hereby increased actomyosin contractility. This happens through a direct interaction and through an indirect pathway where ROCK through myosin phosphatase-Rho interacting protein (MPRIP) inhibition decreases activity of myosin light chain phosphatase (MLCP). Decreased levels of phospho-MPRIP and increased levels of phosphorylated cofilin 1 were found in *PARK2* KO neurons. (C) RhoA activity, measured by the ratio of active GTP-bound RhoA to total RhoA, was significantly increased in *PARK2* KO neurons compared to controls. Mean ± SEM, N = 4 independent differentiations. (D) Western blotting confirmed a significant increase in the level of phospho-cofilin 1 (S3) in *PARK2* KO neurons. Expression levels for phospho-cofilin 1 and total cofilin 1 were normalized to β-actin and the phospho-cofilin 1 (S3) expresseion shown relative to the total cofilin 1 expression per differentiation. Mean ± SEM, N = 3 independent differentiations, Student's t-test. (E) Scratch assay was applied to differentiation day 19 *PARK2* KO and isogenic control neurons to evaluate cell migration. Scratches were imaged initially (day 0) and after 5 days (day 5). The RhoA inhibitor, Rhosin (150 μM), was applied for the duration of the assay. Scale bar = 100 μm. (F) Quantification of the average migration distance of cell nuclei moving into the scratch area, relative to average per differentiation, revealed a significantly increased migration of *PARK2* KO neurons, which was normalized with Rhosin treatment. Mean ± SEM, N = 3 independent differentiations. (G-H) Analysis of the morphology of dopaminergic neuronal precursors: untreated or with three days Rhosin (150 μM) treatment (G) quantifying the average neurite length per neuron (μm) based on (H) immunofluorescence staining of tyrosine hydroxylase (TH, green) staining on differentiation day 13. Scale bar = 50 μm. Mean ± SEM, N = 4–5 wells, data from one differentiation, two-way ANOVA with Tukey's multiple comparison test. *P < .05, **P < .01, ***P < .001. (For interpretation of the references to colour in this figure legend, the reader is referred to the web version of this article.)

increased RhoA activity (Fig. 5B). RhoA signalling has been shown to promote migration of neuronal precursors and inhibit neuritogenesis, an established phenotype in the *PARK2* KO cells (Hall and Lalli, 2010; Sebök et al., 1999). RhoA was expressed by the NSCs and by differentiation day 10 and 25 TUJ1+ and MAP2+ neurons with no apparent differences between *PARK2* KO and control (Fig. S5A-D). However, the RhoA activity, as measured by the ratio of active GTP-bound RhoA out of total RhoA, was significantly increased in *PARK2* KO neurons (Fig. 5C). Correspondingly, Western blotting confirmed a significant increase in the level of cofilin-1 phosphorylated at Ser4, a key site for regulating its activity (Fig. 5D, Fig. S6) (Galkin et al., 2011). To test whether we could detect functional changes in cell migration, we performed a scratch assay on day 19 of the differentiation and assessed the migration of cell bodies into the scratch area after 5 days. *PARK2* KO neurons on average migrated significantly further into the scratch than the healthy isogenic controls (Fig. 5E-F). To test whether increased RhoA signalling could be involved in the enhanced migration, we treated the cells with the RhoA inhibitor, Rhosin, for the duration of the scratch assay. Excitingly, this completely reverted the phenotype, resulting in no difference in migration distance between controls and RhoA inhibitor treated *PARK2* KO neurons (Fig. 5E–F). Tested by two-way ANOVA there was a significant overall effect of *PARK2* KO ($p = .002$) and Rhosin treatment ($p = .007$) with no interaction between the two ($p = .210$).

Furthermore, RhoA inhibition significantly improved the impaired neurite outgrowth documented for day 13 *PARK2* KO TH+ neuronal precursors after just three days of Rhosin treatment (Fig. G-H). Applying two-way ANOVA a significant overall effect of *PARK2* KO ($p < .001$) and Rhosin treatment ($p = .024$), but no interaction between the two ($p = .076$) was present.

In conclusion, we have utilized a mass spectrometry based proteome and PTMome approach to identify novel as well as known phenotypes, including enhanced cell migration and decreased neurite outgrowth in parkin deficient neurons and confirmed these by functional studies, both *in vitro* and *in vivo*. Both cell migration and neurite outgrowth perturbations were reversible with pharmacological inhibition of RhoA signalling.

3. Discussion

To identify functional pathway that changes in PD pathogenesis, we have performed an unbiased large-scale mass spectrometry screen in human iPSC-derived neuronal cultures with and without compound heterozygous *PARK2* mutations. The cultures were not homogenous, but consisted of mainly dopaminergic and GABAergic neurons of varying maturity as well as astrocytes. As dopaminergic neurons do not act in isolation, and functional connections with interneurons and interaction with astrocytes could be of importance for disease modelling, the mixed cultures could be an advantage (Morello and Partanen, 2015; Rappold and Tieu, 2010). Importantly, for all cell identity and –maturity markers examined, the *PARK2* KO and control neurons were identical in their composition. Previously, the *PARK2* KO has been reported to result in a decreased percentage of TH+ neurons (Shaltouki et al., 2015), however in our hands the *PARK2* KO and control NSCs consistently gave rise to identical numbers of TH+ neurons across multiple differentiations. The only difference detected in cell type markers was an increase of about 1% in the levels of GFAP+ astrocytes. GFAP and vimentin levels were, however, almost 1.5-fold increased in *PARK2* KO cultures, where astrocytes with a more complex, hypertrophic morphology were observed. We hypothesize that these changes might be caused by a transition of the *PARK2* KO astrocytes to a more reactive state where GFAP and vimentin are upregulated (Rappold and Tieu, 2010; Sirko et al., 2015), rather than a change in differentiation potential. Increased levels of GFAP in PD brain and enteric nervous system have been interpreted as a sign of reactive astrogliosis (Werner et al., 2008; Clairembault et al., 2014). However, further studies are needed to address the astrocyte reactivity in our cultures.

The proteomics analysis identified large numbers of proteins differentially expressed in *PARK2* KO neurons, four of which we confirmed by Western blotting on samples from independent differentiations, proving the validity and reproducibility of the approach. Changes in these four and other of the most highly up- and down-regulated proteins in the *PARK2* KO neurons, such as Galectin-1, have previously been documented in sporadic PD brains (Werner et al., 2008; Zaltieri et al., 2015; Ambani et al., 1975). Similarly to GFAP, Galectin-1 is upregulated in reactive astrocytes following brain injury and necessary for their proliferation (Sirko et al., 2015).

The finding of protein alterations in our *PARK2* KO iPSC-derived neurons corresponding with changes in sporadic PD brain indicates that common disease processes could be shared between sporadic and *PARK2*-related PD. Parkin dysfunction has been implicated in sporadic PD as a consequence of perturbed solubility following oxidative-, nitrosative- or dopamine-modifications of the protein (Wang et al., 2005; Yao et al., 2004). In addition, parkin dysfunction might be a suitable model of the general mitochondrial dysfunction, which is believed to be a key contributor to sporadic PD pathogenesis.

Our proteomic analysis also incorporated differences in PTMs including phosphorylation and reversible cysteine-modifications, adding valuable information about post-translational regulation of protein function. Reversible cysteine-modifications include S-glutathionylation, S-sulfenation (sulfinic and sulfenic acid), S-nitrosylation and disulfide bond formation, which all serve in cellular defence mechanisms against oxidative stress and numerous signal transduction pathways (Huang et al., 2016; Garcia-Garcia et al., 2012). Recent studies have

demonstrated the importance of protein cysteine oxidation in the regulation of dopaminergic neurodegeneration and mitochondrial activity in PD (Rappold and Tieu, 2010; Sirko et al., 2015; Clairembault et al., 2014).

Whereas the pathway analysis linked the protein level changes to expected functions such as disorder of the basal ganglia and movement disorder, the PTM changes strongly highlighted enrichment of pathways more undescribed in PD including cell migration, neurite outgrowth and RhoA signalling. This underlines the value of examining not only protein levels, but also PTMs in proteomic screening of disease models.

The predicted changes in neuritogenesis and outgrowth were confirmed both *in vitro* and *in vivo*. One earlier study has shown that *PARK2* mutations reduce the complexity of neuronal processes in human iPSC-derived neurons (Ren et al., 2015), which is supported by our findings of decreased neurite length, numbers of neurites and numbers of branch points in the *PARK2* KO dopaminergic neurons. The effect of parkin-dysfunction on neurite outgrowth could be related to mitochondrial dysfunction (Mattson et al., 2008), causing a lack in necessary energy production, but it could also be independent of mitochondrial influence. Parkin has been shown to bind strongly to microtubules, stabilizing their structure and protecting against microtubule-depolymerizing PD toxins such as rotenone (Yang et al., 2005; Ren et al., 2009). The study of *PARK2* KO and isogenic control neurons transplanted to 6-OHDA lesioned rats confirmed that the neurite outgrowth phenotype was not just present in newly formed neurons, but persisted in mature dopaminergic neurons after 16 weeks *in vivo*. Applying the 6-OHDA lesioned model and the specified injection site enabled us to identify and structurally analyse the grafted cells as no intrinsic dopaminergic cell bodies or nigrostriatal TH+ fibers were present. By transplanting neurons to rodent midbrain it is possible to maintain them for prolonged time periods in a more natural and complete microenvironment than what can be obtained *in vitro*. This might prove to be a more optimal solution for determining relevant phenotypic changes caused by genetic risk factors (Korecka et al., 2016).

Neurite outgrowth defects have similarly been established in iPSC-derived neurons from LRRK2 and sporadic PD patients (Sánchez-Danés et al., 2012; Borgs et al., 2016). In PD patients, synaptic and axonal degeneration occurs prior to the loss of neuronal soma in the SN in the human brain (Chu et al., 2012; Burke and O'Malley, 2013). Combined these findings could imply that neurite defects are an important part of early disease processes in PD.

The pathway analysis additionally predicted cell migration to be perturbed in *PARK2* KO neurons, which was confirmed by scratch analysis proving that *PARK2* KO neurons migrated significantly further than the controls. This phenotype has not been reported before in iPSC-derived neurons with *PARK2* or other PD-related genetic mutations. RhoA signalling, which was significantly increased in the *PARK2* KO cultures, has been shown to inhibit neurite outgrowth and promote migration of neuronal precursors fitting with the two main phenotypes documented in our *PARK2* KO neurons (Stankiewicz and Linseman, 2014; Sebök et al., 1999). In our cultures RhoA inhibition could rescue both of these phenotypes, as *PARK2* KO neurons treated with RhoA inhibitor showed similar levels of migration as untreated control cells and RhoA inhibition significantly increased neurite outgrowth. The neurite outgrowth and migration changes were analyzed in dopaminergic neurons and further analyses are needed to determine whether they can be detected in other neuronal subtypes.

The role of RhoA signalling in PD pathogenesis is supported by studies of MPTP-treated mice that show an upregulation in the substantia nigra of RhoA and its downstream target ROCK (Villar-Cheda et al., 2012). Inhibition of ROCK causes a significant decrease in dopaminergic cell death and has been suggested as a neuroprotective strategy in PD (Tönges et al., 2012). Deletion of RhoA from the midbrain leads to increased proliferation of neural progenitor cells and activation of RhoA by various degenerative insults elicits a pro-apoptotic cascade through ROCK (Stankiewicz and Linseman, 2014). The connection between parkin dysfunction and RhoA could be elicited through PI3K/Akt, which was amongst the predicted canonical pathways in our analysis. Parkin depletion results in enhanced PI3K/Akt activation, which in turn increases RhoA signalling (Gupta et al., 2017; Błajecka et al., 2012).

Future studies are needed to examine the exact pathways leading from parkin dysfunction to perturbations neurite outgrowth and migration as well as the role of RhoA signalling in these events. It should be noted that this study was performed using only one set of control and isogenic *PARK2* KO iPSC lines. Although the SNP-array did not identify additional genetic differences between the lines, confirmation of the results using other isogenic iPSC lines with and without *PARK2* mutation is of high relevance. Additionally, verifications of these findings in iPSC-derived neurons from PD patients both with *PARK2* mutations and sporadic disease could clarify the importance of the findings and their potential for future disease-modifying treatments.

In conclusion, our study has revealed that iPSC-derived *PARK2* KO neuronal precursors exhibit distinct phenotypes including increased migration and reduced neurite outgrowth. The GTP-binding protein RhoA was identified as a key upstream regulator, and by inhibiting this pathway the migration and neurite outgrowth phenotypes could be rescued. Our novel findings, which could have implications for potential future treatments, highlight the vast potential of combining iPSC technology and advanced mass spectrometry.

4. Methods

4.1. Ethical statement

The Research Ethics Committee of the Region of Southern Denmark approved the study prior to initiation (S-20130101). All use of laboratory animals was performed in accordance with local animal ethics regulations (University of Southern Denmark) and the rules of the Danish Animal Experiments Inspectorate under license 2012-DY-2934-00008.

4.2. Stem cell lines

The healthy control iPSC line, XCL-1, was generated by XCell Science Inc. (Novato, CA) from CD34+ cord blood cells using episomal vectors for the reprogramming process. The isogenic *PARK2* compound heterozygous KO iPSC line was generated from XCL-1 using zinc finger technology and characterized as described elsewhere (Shaltouki et al., 2015). The mutation was originally described as localised in exon 1 out of ten *PARK2* exons. However, the current consensus is that *PARK2* contains 12 exons of which the reported sequence belongs to exon 2 and we will therefore describe it as such (Shaltouki et al., 2015). The control and *PARK2* KO iPSC lines and corresponding NSC derivatives were obtained from XCell Science Inc. (Novato, CA) (Shaltouki et al., 2015; Swistowski et al., 2009).

4.3. iPSCs and NSCs culture and differentiation

iPSCs and NSCs were characterized and propagated according to standard protocols. iPSC differentiation to NSCs was performed by XCell Science Inc. using a 14 day protocol where iPSCs were initially differentiated in suspension as embryoid bodies followed by formation of attached neural rosettes, isolation and expansion of NSCs from these (Swistowski et al., 2009). Dopaminergic differentiation was achieved by culturing NSCs in DOPA Induction and Maturation Medium (XCell Science) according to manufacturer instructions for at least 25 days. See Supplemental Information for detailed procedures.

4.4. Immunocytochemistry and Western blotting

Immunocytochemistry and Western blotting were performed using standard methods. Detailed descriptions can be found in Supplemental Information.

Primary antibodies were used in the following concentrations:

For immunocytochemistry: rabbit anti-tyrosine hydroxylase (TH, Millipore #AB152) 1:600, mouse anti-TH (Millipore #AB5280) 1:600, mouse anti-β-tubulin-III (Sigma #T8660) 1:2000, mouse anti-microtubule-associated protein 2a + b (MAP2, Sigma #M1406) 1:2000, mouse anti-Human Nuclei (HN, Millipore #MAB1281) 1:500, mouse anti-Oct-3/4 (Santa Cruz #sc-5279) 1:50, goat anti-Sox-2 (Santa Cruz #sc-17,320) 1:50, mouse anti-Nestin (Abcam #OBT1610) 1:500, rabbit anti-GFAP (DAKO #Z0334) 1:4000, mouse anti-NeuN (Millipore #MAB377) 1:500, rabbit anti-GABA (Sigma #A2052), and mouse anti-RhoA (Santa Cruz #SC418) 1:600.

For Western blotting: Mouse anti-β-Actin-HRP (Abcam #49900) 1:50000, mouse anti-Parkin (Cell Signalling #4211) 1:1000, mouse anti-Parkin (Santa Cruz #sc-32,282) 1:500, rabbit anti-Catalase (Cell Signalling #12980) 1:1000, chicken anti-GFAP (Abcam #ab4674) 1:10000, rabbit anti-LC3A (Cell Signalling #4599) 1:1000, rabbit anti-LC3B (Sigma #L7543) 1:1000, rabbit anti-SynapsinIII (Abcam #175533) 1:500, rabbit anti-Vimentin (Abcam #ab92547) 1:1000, mouse anti-RhoA (Santa Cruz #SC418) 1:600, rabbit anti-Cofilin (D3F9) (Cell Signalling #5175) 1:1000 and rabbit anti-phospho-cofilin (S3) (Cell Signalling #3313) 1:1000.

4.5. Mass spectrometry sample collection and protein isolation

Differentiation day 25 neurons from three independent differentiations were collected on ice in phosphate-buffered saline (PBS, ThermoFisher) with protease- (Complete tablets, Roche) and phosphatase inhibitors (PhosSTOP tablets, Roche). Samples were sonicated and incubated for 30 min at RT in lysis buffer consisting of 6 M urea (Sigma), 2 M thiourea (Sigma), 20 mg/ml sodium dodecyl sulfate (SDS, GE Healthcare), 40 nM N-ethylmaleimide (NEM, Sigma) and protease inhibitor.

4.6. Reduction and enzymatic digestion

Following methanol-chloroform precipitation (Sigma), proteins were denatured and reduced in 6 M urea, 2 M thiourea, 10 mM TCEP (ThermoFisher) and 1 μl endoproteinase Lys-C (Wako) at RT for 2 h. The samples were diluted 10 times in 20 mM TCEP and 20 mM triethylammonium bicarbonate (TEAB, Sigma) buffer, pH 7.5 and sonicated followed by digestion with 1 μg trypsin (Sigma) per 50 μg peptide ON at RT.

4.7. Desalting and tandem mass tag labeling

The samples were acidified with trifluoroacidic acid (TFA, Sigma) and desalted using self-made P200-tip-based columns. A small plug of C_{18} material from a 3 M Empore™ disk (Sigma) was inserted in the constricted end of a P200 pipette tip and 1.5 cm of the tip was packed with reversed-phase resin material consisting of a 1:1 mix of Poros 50 R2 (Applied Biosystems) and Oligo R3 (Applied Biosystems) resins dissolved in 100% acetonitrile (ACN, Sigma) by applying air pressure with a 1 ml syringe. The acidified samples were loaded onto the micro-columns and washed with 0.1% TFA. The peptides were eluted using 60% ACN/0.1% TFA and subsequently dried by speed vacuum centrifugation.

Peptide concentrations were measured by Qubit® (Thermo Scientific) and 90 μg of each sample were labeled with Tandem Mass Tag (TMT) Sixplex Isobaric label Reagents (Thermo Scientific) both according to the manufacturer's instructions. Efficient labeling was confirmed by MALDI, and the peptides mixed 1:1:1:1:1:1 and dried.

4.8. Enrichment of phosphorylated and cysteine-modified peptides

Phospho-peptide enrichment and fractionation were essentially performed as earlier described (Engholm-Keller et al., 2012) by using TiO_2, sequential elution from IMAC beads and fractionation by HILIC (TiSH method). Peptides were dissolved in 80% ACN/5%TFA with 1 M glycolic acid (Sigma) and incubated with 0.6 mg titanium dioxide (TiO_2) beads (Titansphere 10 μm, GL Sciences) per 100 μg peptide for 30 min at RT with vigorous shaking. The beads were centrifuged briefly and the supernatant transferred to a new tube with 0.3 mg TiO_2 beads per 100 μg peptide. After 15 min incubation at RT with vigorous shaking and a brief centrifugation the supernatant was collected. The beads were washed with 80% ACN/1% TFA and 10% ACN/0.1% TFA. The supernatant with the unbound TiO_2 fraction and the washing fractions, both containing the non-modified peptides, were combined. The phosphorylated peptides were eluted from the beads by incubation with 1.5% ammonium hydroxide solution (Sigma), pH 11.3, at RT with vigorous shaking. The beads were spun down and the supernatant passed through C_8 material from a 3 M Empore™ disk (Sigma) before the samples were dried.

The dried phosphorylated peptides were dissolved in 20 mM TEAB, reduced with 5 mM dithiothreitol (Sigma) for 30 min at RT and alkylated with 20 mM NEM for 30 min at RT in the dark. To separate out sialylated glyco-peptides that also bind to the TiO_2 beads (Larsen et al., 2007) the sample was deglycosylated with N-glycosidase F (Biolabs) and Sialidase A (Prozyme) at 37 °C ON. The sample was dried, re-suspended in SIMAC loading buffer (50% ACN/0.1% TFA) and incubated with PhosSelect IMAC beads (Sigma), pre-equilibrated in SIMAC loading buffer, for 30 min at RT with gentle shaking. The beads were packed in a constricted p200 GeLoader tip by applying gentle air pressure with a 1 ml syringe and the flow through collected and combined with washing of the beads (IMAC loading buffer) before mono-phosphorylated peptides were eluted with 20% ACN/1% TFA and combined with the washing fraction and dried. The multi-phosphorylated peptides were then eluted with 1.5% ammonium hydroxide solution, pH 11.3, and dried. The mono-phosphorylated and deglycosylated peptides were separated by adjusting the sample to 70% ACN/2% TFA and repeating the TiO_2 bead enrichment as described above (washing with 50% ACN/0.1%TFA).

The dried non-modified sample was desalted on R2/R3 columns as described above and dissolved in 50 mM TEAB and 20 mM TCEP, pH 7, for one hour. The sample was incubated with 10 mM cysteine-specific phosphonate adaptable tag (CysPAT) in house synthesized as previously described (Huang et al., 2016), for 1 h at RT in the dark with gentle shaking. The CysPAT reacts with reversibly modified cysteines and the phosphonate group allows for the subsequent isolation of CysPAT-labeled peptides from non-modified peptides using TiO_2 bead enrichment as earlier detailed.

All the eluates were dried and desalted on self-made columns as described previously, using only R3 material for the mono- and multi-phosphorylated peptides and R2/R3 material for cysteine- and non-modified peptides.

4.9. Hydrophobic interaction liquid chromatography (HILIC) and high pH fractionation

To reduce sample complexity mono-phosphorylated, CysPAT-labeled and non-modified peptides were fractionated using HILIC as described previously (Engholm-Keller et al., 2012). The non-modified sample was first diluted in 0.1% TFA and approximately 50 μg peptide was fractioned. All mono-phosphorylated and CysPAT samples were fractionated. The samples were dissolved in 90% ACN, 0.1% TFA (solvent B) and loaded onto an in-house packed TSKgel Amide-80 (Tosoh Bioscience) micro-capillary column (450 μm OD x 320 μm ID x 17 cm) using an Agilent 1200 Series HPLC (Agilent). Peptides were separated using a gradient from 100 to 60% solvent B (A = 0.1% TFA)

running for 30 min at a flow-rate of 6 µl/min. Fractions were collected every 1 min and combined into 12–15 final fractions based on the UV chromatogram and subsequently dried by vacuum centrifugation.

To increase the coverage of the non-modified peptides, high pH fractionation was also performed using approximately 50 µg peptide. Briefly, the sample was dissolved in 1% ammonium hydroxide (NH_3, Sigma), pH 11, and loaded on a R2/R3 column equilibrated with 0.1% NH_3. The peptides were eluted in a stepwise fashion using a gradient of 5%–60% ACN/0.1% NH_3. All fractions were dried by vacuum centrifugation and stored at −20 °C.

4.10. Reversed-phase nanoLC-ESI-MS/MS

The samples were resuspended in 0.1% formic acid (FA) and loaded onto a two-column EASY-nLC system (Thermo Scientific). The pre-column was a 3 cm long fused silica capillary (100 µM inner diameter) with a fritted end and in-house packed with ReproSil - Pur C18 AQ 5 µm (Dr. Maisch GmbH) whereas the analytical column was a 17 cm long fused silica capillary (75 µm inner diameter) and packed with ReproSil–Pur C18 AQ 3 µm reversed-phase material (Dr. Maisch GmbH).

The peptides were eluted with an organic solvent gradient from 100% phase A (0.1% FA) to 34% phase B (95% ACN, 0.1% FA) at a constant flowrate of 250 nl/min. Depending on the samples based on the HILIC, the gradient was from 1 to 30% solvent B in 60 min or 90 min, 30% to 50% solvent B in 10 min, 50%–100% solvent B in 5 min and 8 min at 100% solvent B.

The nanoLC (nLC) was online connected to a QExactive HF Mass Spectrometer (Thermo Scientific) operated at positive ion mode with data-dependent acquisition. The Orbitrap acquired the full MS scan with an automatic gain control target value of 3×10^6 ions and a maximum fill time of 100 ms. Each MS scan was acquired at high-resolution (120,000 full width half maximum (FWHM)) at *m/z* 200 in the Orbitrap with a mass range of 400–1400 Da. The 12 most abundant peptide ions were selected from the MS for higher energy collision-induced dissociation (HCD) fragmentation (collision energy: 34 V). Fragmentation was performed at high resolution (60,000 FWHM) for a target of 1×10^5 and a maximum injection time of 60 ms using an isolation window of 1.2 m/z and a dynamic exclusion. All raw data were viewed in Thermo Xcalibur v3.0.

4.11. Mass spectrometry data analysis

The raw data were processes using Proteome Discoverer (v2.2, ThermoFisher) and searched against the Swissprot human database using an in-house Mascot server (v2.3, Matrix Science Ltd.).

Database searches were performed with the following parameters: precursor mass tolerance of 10 ppm, fragment mass tolerance of 0.05 Da (HCD fragmentation), TMT 6-plex (Lys and N-terminal) as fixed modifications and a maximum of 2 missed cleavages for trypsin. Variable modifications were NEM on Cys along with phosphorylation of Ser/Thr/Tyr and N-Succinimidyl iodoacetate on Cys for the phosphorylated and CysPAT-modified groups, respectively. Only peptides with up to a q-value of 0.01 (Percolator), Mascot rank 1 and cut-off value of Mascot score > 15 were considered for further analysis. Only proteins with more than one unique peptide were considered for further analysis in the non-modified group. The relative abundances of modified peptides (phosphorylated and cysteine-modified peptides) were normalized by the protein expression to distinguish differential regulated modifications from altered protein expression (Wu et al. 2011). The Rank products test was applied to identify significant expression changes for proteins and PTMs using a q-value (false discovery rate (FDR)-adjusted *p*-value) of 0.05 and 0.1, respectively (Schwämmle et al., 2013).

The mass spectrometry proteomics data have been deposited to the ProteomeXchange Consortium *via* the PRIDE partner repository with the dataset identifier PXD007871 and can be accessed with the username: reviewer26947@ebi.ac.uk and password: rlcurSin (Vizcaíno et al., 2016).

The pathway analysis was performed using the Ingenuity Pathway Analysis software (IPA, QIAGEN) on the three datasets; the differentially regulated non-modified-, phosphorylated and cysteine-modified proteins. Direct and indirect relationships, either experimentally observed or highly predicted based on data from CNS tissue or cell lines, were included. The IPA comparison analysis was used to combine results from all three datasets and rank the most significantly enriched pathways according to the IPA calculated z-score.

4.12. Striatal dopamine depletion and transplantation procedure

Female Sprague-Dawley rats (Taconic, Denmark), weighing 180–220 g, were anesthetized using fentanyl citrate 236 µg/kg and fluanisone 7.5 mg/kg (Hypnorm, VetaPharma Ltd., UK) and midazolam 3.75 mg/kg (Hameln Pharmaceuticals Ltd., Germany) injected subcutaneously (SC). Striatal dopamine depletion was performed with a stereotaxic device (Kopf Instruments, USA) by injection of 4 µl 6-hydroxydopamine (6-OHDA) solution consisting of 32 mM 6-OHDA (Sigma), 1% ascorbic acid (Sigma) and 0.9% NaCl (B. Braun, Germany) into the right ascending mesostriatal pathway. The injection was performed over 6 min using a 5 µl Hamilton (Variant 75RN, Sigma) microsyringe fitted with a 26 s gage blunt tip needle inserted through a small burr hole with the following coordinates relative to bregma: A/P + 2.8, M/L + 2.0, D/V -8.4 from dura mater and tooth bar −3.9.

Lesions were evaluated using the amphetamine-induced rotation test. The rats were injected intraperitoneally (IP) with 2.5 mg/kg D-amphetamine (Sygehusapotek OUH, DK) and their rotational behaviour monitored for 120 min with a rotometer system (RotoRat Test Station, MED Associates Inc., USA). Analysis was performed on the last 90 min and the net rotational asymmetry score measured as full body turns per min. Only rats exhibiting a mean ipsilateral rotation score of at least four, were included in the study and divided, according to rotation scores, into two balanced groups ($N = 16$ rats/group, sample size based on earlier comparable studies).

Transplantation of *PARK2* KO and control neuronal precursors was performed by the same procedure as described for the 6-OHDA lesions with the operators blinded to cell type. Differentiation day 16–17 cells were treated with accutase for 5 min, centrifuged at 300 *g* for 4 min and resuspended in DMEM (ThermoFisher). 3 µL cell suspension with 4×10^6 cells was stereotactically injected over 6 min into the striatum of the rats using the following coordinates relative to bregma: A/P + 0.55, M/L + 3.0, D/V -4.5 from dura mater and tooth bar −2.4 mm. After injection, the needle was slowly retracted (1 mm/min). The rats were immunosuppressed with daily IP injections of 10 mg/kg Prednisolon (Sygehusapotek OUH, DK) from three days before till ten days after transplantation, and every second day SC injections of 20 mg/kg Cyclosporine A (Sygehusapotek OUH, DK) from three days before transplantation until termination.

4.13. Histological processing and immunohistochemistry

16 weeks posttransplantation, the rats were anesthetized and PFA-perfused for histological processing of their brains. See Supplemental Information for detailed procedures.

4.14. Neurite outgrowth in vitro and in vivo

Morphological analysis was performed on immunostained TH+ cells using the NeuronJ plugin for ImageJ (Meijering et al., 2004). The analysis was performed investigator-blinded on *in vitro* differentiation day 13 cells with and without three days treatment with the RhoA GTPase inhibitor, Rhosin (Tocris) at 150 µM and *in vivo* transplanted cells. The numbers of primary neurites and branch points, the size of the soma as well as the length of the neurites were quantified. Only cells

with intact soma and one or more neurites were included. For measurements of neurite length and branch points overlapping neurites were excluded.

4.15. Scratch assay

Cell migration was evaluated *in vitro* using the scratch assay. Control and *PARK2* KO neuronal precursors were replated in 24-well plates at differentiation day 10 and at day 19 a scratch was applied in the center of each well using a sterile 2 mm-wide steel spatula. Rhosin treatment (Tocris) at 150 μM was initiated at day 19 and replenished every second day with medium change. The scratches were imaged daily using an automated DMI4000B microscope (Leica) until day 24, before they were fixed and immunostained for TH and HN. The number of cell bodies migrating into the scratch and the migration distance for each cell was quantified using ImageJ with the investigator blinded.

4.16. RhoA activity

The ratio of active, GTP-bound RhoA to total RhoA was determined using the G-LISA RhoA Activation Assay Biochem Kit (Cytoskeleton Inc.) according to manufacture instructions. Total RhoA was determined using Western blotting as described above.

4.17. Statistical analysis

Analysis was performed in Microsoft Excel or Graphpad Prism version 5.0 (GraphPad Software, USA) using two-tailed unpaired Student's *t*-tests with or without Welch's correction and two-way ANOVA with Tukey's Multiple Comparison Test where appropriate. Results are expressed as mean ± SEM, and p-values < .05 were considered statistically significant.

Author contributions

H.B., P.J., M.R.L., and M.M. designed research; H.B., P.J., M.A., M.R., J.O., S.S., P.N., C.F., and J.G. performed research; X.Z., L.R., and R.W.M. contributed new reagents or analytic tools; H.B., P.J., J.O., M.A., M.R., S.S., B.R. and J.G. analyzed data; H.B., B.R., and M.M. wrote the paper.

Declaration of Competing Interest

The authors declare that they have no conflict of interest.

Acknowledgements

The authors would like to thank Dorte Lyholmer, Ulla Melchior Hansen, Honggang Huang and Taewook Kang for technical assistance. This work was supported by (grant number): the Innovation Fund Denmark (BrainStem; 4108-00008A), the Lundbeck Foundation (R167-2013-15778), the Danish Parkinson Foundation, the Jascha Foundation (3687, 5611), IMK Almene Fond, the A.P. Møller Foundation for the Advancement of Medical Science (15-396, 14-427), Knud og Edith Eriksens Mindefond, Frimodt-Heineke Fonden, and Carl og Ellen Hertz Legat and the Faculty of Health Sciences, University of Southern Denmark.

The bioimaging experiments reported in this paper were performed at DaMBIC, a bioimaging research core facility, at the University of Southern Denmark. DaMBIC was established by an equipment grant from the Danish Agency for Science Technology and Innovation and by internal funding from the University of Southern Denmark. The Villum Center for Bioanalytical Sciences at SDU is acknowledged for access to advanced Mass Spectrometric instrumentation.

Appendix A. Supplementary data

Supplementary data to this article can be found online at https://doi.org/10.1016/j.nbd.2019.104581.

References

Abou-Sleiman, P.M., Muqit, M.M.K., Wood, N.W., 2006. Expanding insights of mitochondrial dysfunction in Parkinson's disease. Nat. Rev. Neurosci. 7, 207–219.
Ambani, L.M., Van Woert, M.H., Murphy, S., 1975. Brain peroxidase and catalase in Parkinson disease. Arch. Neurol. 32, 114–118.
Barrett, P.J., Timothy Greenamyre, J., 2015. Post-translational modification of α-synuclein in Parkinson's disease. Brain Res. 1628, 247–253.
Beilina, A., Cookson, M.R., 2016. Genes associated with Parkinson's disease: regulation of autophagy and beyond. J. Neurochem. 139 (Suppl. 1), 91–107.
Błajecka, K., et al., 2012. Phosphoinositide 3-kinase C2β regulates RhoA and the actin cytoskeleton through an interaction with Dbl. PLoS One 7, e44945.
Bonifati, V., et al., 2003. Mutations in the DJ-1 gene associated with autosomal recessive early-onset parkinsonism. Science 299, 256–259.
Borgs, L., et al., 2016. Dopaminergic neurons differentiating from LRRK2 G2019S induced pluripotent stem cells show early neuritic branching defects. Sci. Rep. 6, 33377.
Burke, R.E., O'Malley, K., 2013. Axon degeneration in Parkinson's disease. Exp. Neurol. 246, 72–83.
Choi, J., et al., 2004. Oxidative modifications and down-regulation of ubiquitin carboxyl-terminal hydrolase L1 associated with idiopathic Parkinson's and Alzheimer's diseases. J. Biol. Chem. 279, 13256–13264.
Chu, Y., et al., 2012. Alterations in axonal transport motor proteins in sporadic and experimental Parkinson's disease. Brain 135, 2058–2073.
Chung, S.Y., et al., 2016. Parkin and PINK1 patient iPSC-derived midbrain dopamine neurons exhibit mitochondrial dysfunction and α-synuclein accumulation. Stem Cell Rep. 7, 664–677.
Clairembault, T., et al., 2014. Enteric GFAP expression and phosphorylation in Parkinson's disease. J. Neurochem. 130, 805–815.
Danielson, S.R., et al., 2011. Quantitative mapping of reversible mitochondrial complex I cysteine oxidation in a Parkinson disease mouse model. J. Biol. Chem. 286, 7601–7608.
Dawson, T.M., Dawson, V.L., 2014. Parkin plays a role in sporadic Parkinson's disease. Neurodegener. Dis. 13, 69–71.
Dias, V., Junn, E., Mouradian, M.M., 2013. The role of oxidative stress in Parkinson's disease. J. Park. Dis. 3, 461–491.
Engholm-Keller, K., et al., 2012. TiSH–a robust and sensitive global phosphoproteomics strategy employing a combination of TiO2, SIMAC, and HILIC. J. Proteome 75, 5749–5761.
Exner, N., Lutz, A.K., Haass, C., Winklhofer, K.F., 2012. Mitochondrial dysfunction in Parkinson's disease: molecular mechanisms and pathophysiological consequences. EMBO J. 31, 3038–3062.
Fang, J., Nakamura, T., Cho, D.-H., Gu, Z., Lipton, S.A., 2007. S-nitrosylation of peroxiredoxin 2 promotes oxidative stress-induced neuronal cell death in Parkinson's disease. Proc. Natl. Acad. Sci. 104, 18742–18747.
Fernandes, H.J.R., et al., 2016. ER stress and autophagic perturbations lead to elevated extracellular α-synuclein in GBA-N370S Parkinson's iPSC-derived dopamine neurons. Stem Cell Rep. 6, 342–356.
Galkin, V.E., et al., 2011. Remodeling of actin filaments by ADF/cofilin proteins. Proc. Natl. Acad. Sci. U. S. A. 108, 20568–20572.
Garcia-Garcia, A., Zavala-Flores, L., Rodriguez-Rocha, H., Franco, R., 2012. Thiol-redox signaling, dopaminergic cell death, and Parkinson's disease. Antioxid. Redox Signal. 17, 1764–1784.
Gupta, A., et al., 2017. PARK2 depletion connects energy and oxidative stress to PI3K/Akt activation via PTEN S-nitrosylation. Mol. Cell 65 999-1013.e7.
Hall, A., Lalli, G., 2010. Rho and Ras GTPases in axon growth, guidance, and branching. Cold Spring Harb. Perspect. Biol. 2.
Huang, H., et al., 2016. Simultaneous enrichment of cysteine-containing peptides and phosphopeptides using a cysteine-specific phosphonate adaptable tag (CysPAT) in combination with titanium dioxide (TiO2) chromatography. Mol. Cell. Proteomics MCP 15, 3282–3296.
Imaizumi, Y., et al., 2012. Mitochondrial dysfunction associated with increased oxidative stress and α-synuclein accumulation in PARK2 iPSC-derived neurons and postmortem brain tissue. Mol. Brain 5, 35.
Jiang, H., et al., 2012. Parkin controls dopamine utilization in human midbrain dopaminergic neurons derived from induced pluripotent stem cells. Nat. Commun. 3, 668.
Kitada, T., Tong, Y., Gautier, C.A., Shen, J., 2009. Absence of nigral degeneration in aged parkin/DJ-1/PINK1 triple knockout mice. J. Neurochem. 111, 696–702.
Korecka, J.A., Levy, S., Isacson, O., 2016. In vivo modeling of neuronal function, axonal impairment and connectivity in neurodegenerative and neuropsychiatric disorders using induced pluripotent stem cells. Mol. Cell. Neurosci. 73, 3–12.
Labandeira-Garcia, J.L., et al., 2015. Rho kinase and dopaminergic degeneration: a promising therapeutic target for Parkinson's disease. Neurosci. Rev. J. Bringing Neurobiol. Neurol. Psychiatry 21, 616–629.
Lai, Y.-C., et al., 2015. Phosphoproteomic screening identifies Rab GTPases as novel downstream targets of PINK1. EMBO J. 34, 2840–2861.
Larsen, M.R., Thingholm, T.E., Jensen, O.N., Roepstorff, P., Jørgensen, T.J.D., 2005. Highly selective enrichment of phosphorylated peptides from peptide mixtures using titanium dioxide microcolumns. Mol. Cell. Proteomics MCP 4, 873–886.
Larsen, M.R., Jensen, S.S., Jakobsen, L.A., Heegaard, N.H.H., 2007. Exploring the

sialiome using titanium dioxide chromatography and mass spectrometry. Mol. Cell. Proteomics MCP 6, 1778–1787.
Licker, V., et al., 2014. Proteomic analysis of human substantia nigra identifies novel candidates involved in Parkinson's disease pathogenesis. Proteomics 14, 784–794.
Lücking, C.B., et al., 2000. Association between early-onset Parkinson's disease and mutations in the parkin gene. N. Engl. J. Med. 342, 1560–1567.
Mattson, M.P., Gleichmann, M., Cheng, A., 2008. Mitochondria in neuroplasticity and neurological disorders. Neuron 60, 748–766.
Mazzulli, J.R., et al., 2016. Activation of β-Glucocerebrosidase reduces pathological α-Synuclein and restores lysosomal function in Parkinson's patient midbrain neurons. J. Neurosci. 36, 7693–7706.
Meijering, E., et al., 2004. Design and validation of a tool for neurite tracing and analysis in fluorescence microscopy images. Cytom. Part J. Int. Soc. Anal. Cytol. 58, 167–176.
Morello, F., Partanen, J., 2015. Diversity and development of local inhibitory and excitatory neurons associated with dopaminergic nuclei. FEBS Lett. 589, 3693–3701.
Narendra, D., Tanaka, A., Suen, D.-F., Youle, R.J., 2008. Parkin is recruited selectively to impaired mitochondria and promotes their autophagy. J. Cell Biol. 183, 795–803.
Oliveras-Salvá, M., Van Rompuy, A.-S., Heeman, B., Van den Haute, C., Baekelandt, V., 2011. Loss-of-function rodent models for parkin and PINK1. J. Park. Dis. 1, 229–251.
Parri, M., et al., 2007. EphrinA1 activates a Src/focal adhesion kinase-mediated motility response leading to rho-dependent Actino/myosin contractility. J. Biol. Chem. 282, 19619–19628.
Porton, B., Wetsel, W.C., Kao, H.-T., 2011. Synapsin III: role in neuronal plasticity and disease. Semin. Cell Dev. Biol. 22, 416–424.
Rappold, P.M., Tieu, K., 2010. Astrocytes and therapeutics for Parkinson's disease. Neurother. J. Am. Soc. Exp. Neurother. 7, 413–423.
Ren, Y., Zhao, J., Feng, J., 2003. Parkin binds to alpha/beta tubulin and increases their ubiquitination and degradation. J. Neurosci. 23, 3316–3324.
Ren, Y., Jiang, H., Yang, F., Nakaso, K., Feng, J., 2009. Parkin protects dopaminergic neurons against microtubule-depolymerizing toxins by attenuating microtubule-associated protein kinase activation. J. Biol. Chem. 284, 4009–4017.
Ren, R.-J., Dammer, E.B., Wang, G., Seyfried, N.T., Levey, A.I., 2014. Proteomics of protein post-translational modifications implicated in neurodegeneration. Transl. Neurodegener. 3, 23.
Ren, Y., et al., 2015. Parkin mutations reduce the complexity of neuronal processes in iPSC-derived human neurons. Stem Cells Dayt. Ohio 33, 68–78.
Saito, Y., 2014. Oxidized DJ-1 as a possible biomarker of Parkinson's disease. J. Clin. Biochem. Nutr. 54, 138–144.
Sánchez-Danés, A., et al., 2012. Disease-specific phenotypes in dopamine neurons from human iPS-based models of genetic and sporadic Parkinson's disease. EMBO Mol. Med. 4, 380–395.
Schwämmle, V., León, I.R., Jensen, O.N., 2013. Assessment and improvement of statistical tools for comparative proteomics analysis of sparse data sets with few experimental replicates. J. Proteome Res. 12, 3874–3883.
Sebök, A., et al., 1999. Different roles for RhoA during neurite initiation, elongation, and regeneration in PC12 cells. J. Neurochem. 73, 949–960.
Shaltouki, A., et al., 2015. Mitochondrial alterations by PARKIN in dopaminergic neurons using PARK2 patient-specific and PARK2 knockout isogenic iPSC lines. Stem Cell Rep. 4, 847–859.
Sirko, S., et al., 2015. Astrocyte reactivity after brain injury-: the role of galectins 1 and 3. Glia 63, 2340–2361.
Sliter, D.A., et al., 2018. Parkin and PINK1 mitigate STING-induced inflammation. Nature 561, 258–262.
Soldner, F., et al., 2011. Generation of isogenic pluripotent stem cells differing exclusively at two early onset Parkinson point mutations. Cell 146, 318–331.
Stankiewicz, T.R., Linseman, D.A., 2014. Rho family GTPases: key players in neuronal development, neuronal survival, and neurodegeneration. Front. Cell. Neurosci. 8.
Surks, H.K., Richards, C.T., Mendelsohn, M.E., 2003. Myosin phosphatase-rho interacting protein a new member of the myosin phosphatase complex that directly binds RhoA. J. Biol. Chem. 278, 51484–51493.
Swistowski, A., et al., 2009. Xeno-free defined conditions for culture of human embryonic stem cells, neural stem cells and dopaminergic neurons derived from them. PLoS One 4, e6233.
Takeuchi, S., Katoh, H., Negishi, M., 2015. Eph/ephrin reverse signalling induces axonal retraction through RhoA/ROCK pathway. J. Biochem. (Tokyo) 158 (245–252).
Tenreiro, S., Eckermann, K., Outeiro, T.F., 2014. Protein phosphorylation in neurodegeneration: friend or foe? Front. Mol. Neurosci. 7.
Tönges, L., et al., 2012. Inhibition of rho kinase enhances survival of dopaminergic neurons and attenuates axonal loss in a mouse model of Parkinson's disease. Brain J. Neurol. 135, 3355–3370.
Valente, E.M., et al., 2004. Hereditary early-onset Parkinson's disease caused by mutations in PINK1. Science 304, 1158–1160.
Villar-Cheda, B., et al., 2012. Involvement of microglial RhoA/rho-kinase pathway activation in the dopaminergic neuron death. Role of angiotensin via angiotensin type 1 receptors. Neurobiol. Dis. 47, 268–279.
Vizcaíno, J.A., et al., 2016. 2016 update of the PRIDE database and its related tools. Nucleic Acids Res. 44, D447–D456.
Wang, C., et al., 2005. Stress-induced alterations in parkin solubility promote parkin aggregation and compromise parkin's protective function. Hum. Mol. Genet. 14, 3885–3897.
Werner, C.J., Heyny-von Haussen, R., Mall, G., Wolf, S., 2008. Proteome analysis of human substantia nigra in Parkinson's disease. Proteome Sci. 6, 8.
Wu, R., et al., 2011. Correct interpretation of comprehensive phosphorylation dynamics requires normalization by protein expression changes. Mol Cell Proteomics 10 (8).
Yang, F., et al., 2005. Parkin stabilizes microtubules through strong binding mediated by three independent domains. J. Biol. Chem. 280, 17154–17162.
Yao, D., et al., 2004. Nitrosative stress linked to sporadic Parkinson's disease: S-nitrosylation of parkin regulates its E3 ubiquitin ligase activity. Proc. Natl. Acad. Sci. U. S. A. 101, 10810–10814.
Zaltieri, M., et al., 2015. α-synuclein and synapsin III cooperatively regulate synaptic function in dopamine neurons. J. Cell Sci. 128, 2231–2243.